

## Plasma Transfer Arc Additive Manufacturing of 17-4 PH: Assessment of Defects

Sandy El Moghazi<sup>1</sup>, Tonya Wolfe<sup>2</sup>, Douglas G. Ivey<sup>1</sup>, Hani Henein<sup>1</sup>

<sup>1</sup>University of Alberta, Edmonton, Alberta, <sup>2</sup>Innotech Alberta, Edmonton, Alberta

(Corresponding author's email: [ibrahim5@ualberta.ca](mailto:ibrahim5@ualberta.ca))

### Abstract

Plasma transferred arc additive manufacturing is a growing technology in the additive manufacturing world. The Plasma transferred arc additive manufacturing system's ability to produce large samples, compared with other common additive manufacturing techniques, makes it highly desirable in many industrial applications. The selected material in this additive process is 17-4 precipitation hardened stainless steel, which is widely used in numerous fields, such as the aerospace, chemical and mining industries. However, two types of voids were found in the deposits and these voids are detrimental to the mechanical properties. The identified voids were oxide layers and porosity. The presence of oxide layers was correlated to the interaction of atmospheric oxygen with the chromium present in the stainless steel. A shielding hood was designed to provide continuous shielding with inert gas to prevent oxide layer formation. The other source of voids was attributed to the porosity in the initial powders and to the choice of welding process parameters. Changing the powder supplier and optimizing the process parameters, mainly by increasing the heat input to ensure complete melting of the powders, greatly reduced the amount of porosity in the finished part. Hardness measurements were obtained from multiple samples. Hardness was only affected by the ageing process, during which copper precipitates formed within the 17-4 precipitation hardened stainless steel matrix. X-ray diffraction and transmission electron microscopy analyses were conducted to characterize the martensitic matrix before and after the heat treatment and to view copper precipitation after the heat treatment. It is demonstrated that an operating solution to avoid oxide formation is the use of 5% hydrogen in the shield, center and powder gas feeds.

Keywords: Plasma Transferred Arc; Additive Manufacturing; 17-4PH Stainless Steel; Voids; Oxide Layer; Porosity; Hardness

### 1. Introduction

Additive manufacturing (AM) is a rapidly growing manufacturing technology, where the production of complex 3D shapes is attained by a process of layer-by-layer deposition [1,2]. The freedom of design, ability to manufacture complex shapes and the variety of materials that can be used make AM a very desirable manufacturing technique in numerous industries [1]. The parts are produced to a near-net shape once the process is completed.

## 1.1 Material Printed: 17-4PH Stainless Steel

17-4 precipitation hardened (PH) stainless steel, a martensitic stainless steel, has attracted significant attention in many industries due to its excellent corrosion resistance, ease of fabrication and relatively high strength [3–5]. Its corrosion resistance is mainly attributed to the chromium content, while its high strength is due to the precipitation of fine copper precipitates in its martensitic matrix [6]. The heat treatment cycle of 17-4PH stainless steel leads to its strength, hardness and microstructure (Figure 1) [7]. The alloy is initially austenitized at a temperature of 1040°C, where any copper precipitates dissolve in the matrix [6]. The solid solution is then quenched to room temperature, supersaturating the copper in the matrix and giving an average hardness between 250 and 300 Hv [6,8,9]. To increase strength and hardness of the 17-4PH stainless steel, an ageing heat treatment is needed to precipitate the copper. Depending on the desired mechanical properties of the alloy, the temperature and time of the heat treatment are varied. A heat treatment at 480°C for 1 h delivers the highest hardness values, due to optimal ageing of the copper precipitates [6]. This optimum heat treatment results in a tensile strength of approximately 1300 MPa, elongation of 9% and hardness of 450 Hv. [6,10], [11]. Increasing the temperature to a range between 500 and 600°C for 1 h produces a notable reduction in the hardness of the 17-4PH stainless steel, with an increase in ductility. This is attributed to overageing of the copper precipitates, which considerably coarsen at higher heating temperatures, and further tempering of the martensitic matrix [6] [8].

The main microstructural changes that occur during the heat treatment are the precipitation of copper and the transformation of the matrix from lath martensite to tempered martensite [6,10]. The hardness values before and after the optimum ageing process were compared and verified the effect of the copper precipitates on increasing the hardness, as will be discussed below. Changes in the cooling rates affect the resultant microstructure and precipitation of copper. The cooling rates reported in AM can be much faster than those in casting, resulting in microstructures that are very different than those achieved through traditional processing [12]. Therefore, controlling the process parameters in AM is important as this determines the final microstructure and mechanical properties of the alloy.

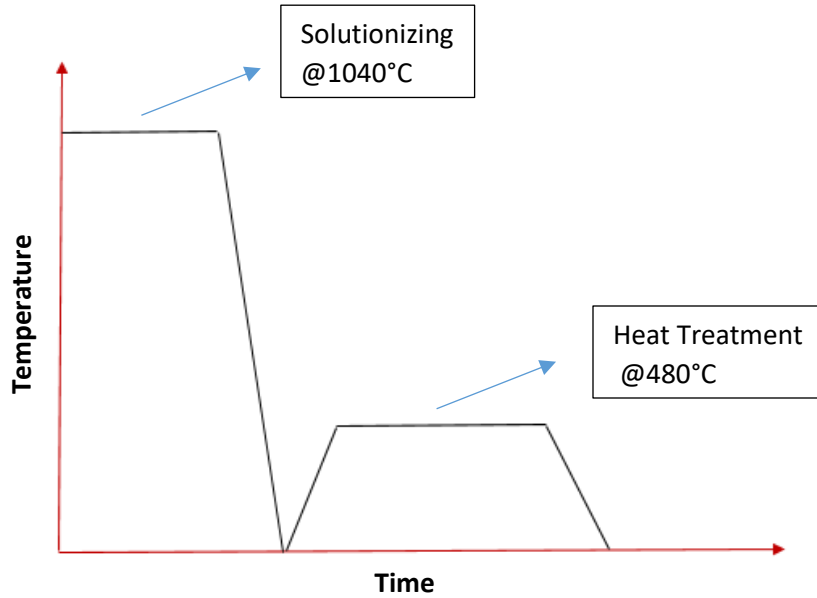


Figure 1 Heat treatment curve of 17-4PH stainless steel.

## 1.2 AM and PTA-AM

Typically, metal AM parts are manufactured using laser or electron beam welding. Recently, however, there has been an interest in adapting arc welding processes to AM due to their high productivity as compared with laser processes. Among the arc welding processes, plasma transferred arc is of particular interest. Its lower heat input and good productivity make it an excellent candidate for AM [13]. Plasma transferred arc welding (PTAW) is widely used for overlay welding to enhance the wear resistance of surfaces used in highly corrosive environments. This is achieved by the deposition of a protective abrasion/corrosion resistant layer on the surface of the part [14]. Compared with other overlaying techniques, such as thermal spraying, PTAW offers higher deposition rates, thicker overlays, good deposition efficiency and relatively lower dilution of the base material [15]. For the aforementioned reasons, a plasma transferred arc additive manufacturing (PTA-AM) machine has been developed to additively manufacture whole parts for industries like the energy sector, in particular oil sands mining. By doing so, many costly hours of unplanned operational shutdown waiting for part replacements can be eliminated and more complex parts can be manufactured that will yield operational improvements. When compared with laser and electron beam AM, PTA-AM is highly desirable as a cost effective solution for larger industrial applications. Fabricating AM parts using PTA-AM allows for faster production of larger parts when compared with laser and electron beam AM. Additionally, because PTA-AM has multiple powder hoppers, it is not limited to producing parts with just a single material; composite materials and gradations between two or more materials can be achieved [2,13].

Powder bed fusion (PBF) AM processes, including laser and electron beam, have successfully fabricated parts using 17-4PH stainless steel. The studies behind these experiments sought a general understanding

of the influence of the separate processing parameters on the properties of the final 17-4 PH stainless steel part. Issues of interest include density, hardness and defects [7]. The general findings from those processes indicated that defects such as porosity and lack of fusion (LOF) defects were common, especially in processes like powder bed fusion [16] [17]. Samples printed using the PTA-AM system had the same types of general defects, as will be discussed in this paper. Porosity is also a common finding when casting 17-4PH stainless steel and, likewise, can be attributed to the processing parameters during casting. Both shrinkage porosity and gas porosity can be eliminated by optimizing process parameters such as the casting temperature, design of cast and solidification time [18]. It can be concluded that defects found in the AM parts while printing 17-4PH stainless steel using the PTA-AM system were common findings in other AM processes and not specific to the PTA-AM process.

Figure 2 shows a photograph of the PTA-AM system at InnoTech Alberta. The powders are delivered in an inert gas medium from the hopper to the torch. Inert gas (argon) is required for the center, powder and shield gases during the welding process. A high current ionizes the inert gas that is fed into the torch system and transforms it into a plasma. The plasma generates very high temperatures that melt the feed alloy powder which then deposit on a substrate [2]. The properties of the final product are highly dependent on the alloy used and the process parameters during deposition [1,13,19]. Furthermore, the effect of different thermal histories on the deposited AM part allows for more anisotropy in the parallel and perpendicular directions during deposition. As such, the controllable process parameters and the quality and properties of the material play crucial roles in the microstructure and thus the mechanical properties of the final product.

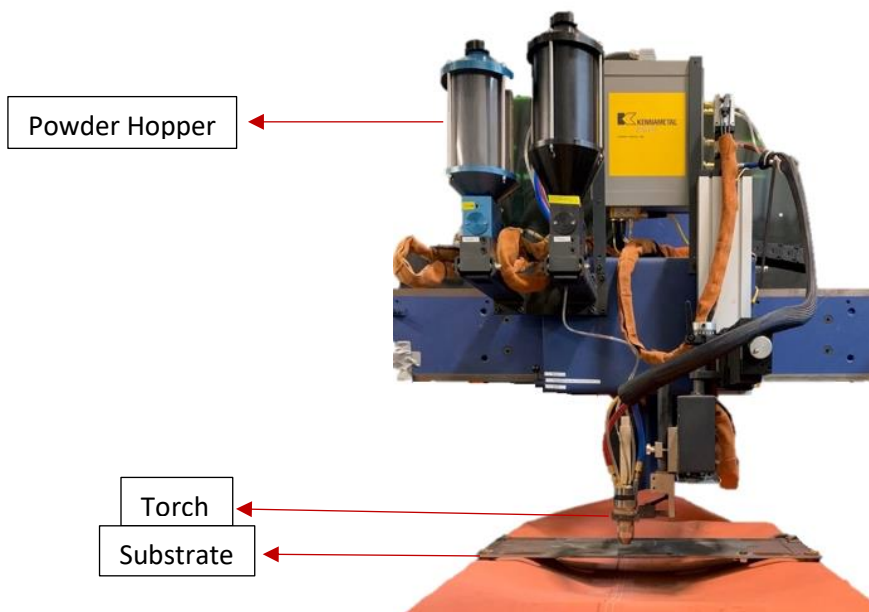


Figure 2 Photograph of the PTA-AM system at InnoTech Alberta.

### 1.3 AM Process Defects

AM processing is a highly competitive and attractive field. Like any growing field of interest, AM parts have associated process defects that need mitigation. In AM, some of the defects appear as voids. The first type of defect observed in fabricated samples of 17-4PH stainless steel is associated with the formation of oxide layers between the interlayers of AM [20]. The formation of oxide layers is not common to all AM processes; it is more specific to direct energy deposition (DED) processes due to the lack of a continuous inert gas environment over the whole AM surface as it is being fabricated. The type of stainless steel used in any application is dependent on the corrosion resistance that is required and, hence, determines the necessary chromium content in the stainless steel. To achieve the desired corrosion resistance, a thin chromium oxide layer forms on the surface of the steel sample to isolate the stainless steel from corrosion and environmental degradation [21]. Hence, most stainless steels are very reactive during processing and must be shielded from the atmosphere when using an AM-DED process. In addition to voids formed due to oxide layers, porosity has been detected as the second type of defect. Pore formation in AM parts has been reported for different processes. For example, hatch speed and hatch spacing were found to directly affect the amount of porosity present in direct metal laser sintered (DMLS) parts) [22].

Porosity found by Fayazfar et al. originated from two sources: gas porosity or LOF porosity [23]. The first type is induced by the absorption of atmospheric gases such as nitrogen, oxygen or hydrogen in the liquid pool [24]. The second type forms as voids around non-fully melted powders during the solidification process [23]. Both types of porosity can be detrimental to the longevity of the produced AM part, since porosity has been identified as a major cause of crack propagation in AM samples [16]. Additionally, porosity present in the initial powders is another detrimental cause of porosity in the final part, as will be discussed later.

Solidification shrinkage, alongside porosity, is another detrimental feature in AM parts. During the deposition of molten droplets over the previous solidifying layer, or the cooler substrate, anisotropic shrinkage occurs between the layers of the AM part. The dissimilar thermal gradients between the deposited layers lead to substantial overall thermal stresses, which can result in premature failure [25]. The present paper will, however, only focus on the former of the mentioned AM issues; namely, void formation due to oxide layers and porosity due to initial powders and LOF.

While research has been conducted on each of the above issues, no previous research has been found addressing the fabrication of 17-4PH stainless steel using PTA-AM. The focus of this paper is to explore different experimental methodologies to alleviate the issues of oxide layer and pore formation in the AM part of 17-4PH stainless steel using PTA-AM.

## 2. Experimental Procedures

## 2.1 Description of the PTA-AM System

An image of the PTA-AM system used in this study is shown in Figure 2. It is integrated with a 3-axis motion linear drive table, which allows for the production of more complex AM designs [13]. The integrated system is able to control most of the parameters in this process, such as movement direction, shield gas, powder gas and center gas flow rates, powder feed rate, current, voltage and coordinated travel speed. The commercial PTA system is a Kennametal Starweld 400 PTA Welding system, with a Kennametal Stellite Excalibur Torch. An image of the torch is presented in Figure 3 where the nozzle of the center gas, powder gas and shield gas are presented alongside the non-consumable tungsten electrode. It is important to note that the torch provides a shielding atmosphere around the powder being deposited; however, it is localized to the area directly beneath the torch. The PTA-AM geometry is created by defining a set of parameters, from the aforementioned controllable parameters, by inputting them into the machine's control pendant. The control pendant is the interface between the user and the PTA-AM system. It allows for the selection and control of all the process parameters during the printing process.

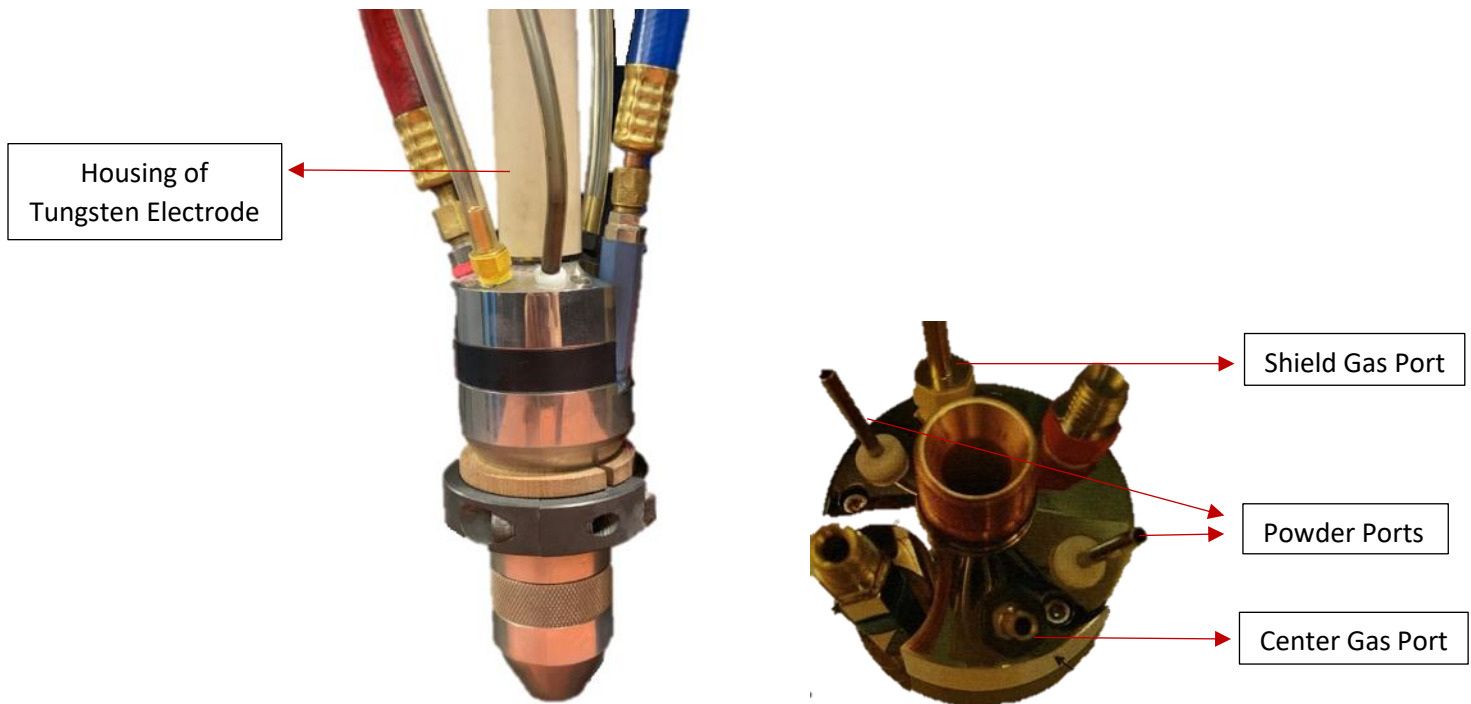


Figure 3 Front view (left) and top view (right) of Kennametal Stellite Excalibur Torch.

## 2.2 Shielding Hood Design

To generate a protective, inert atmosphere over the entire AM part while it was being fabricated, a shielding hood was designed, constructed and installed around the torch (Figure 4). This ensured that the deposited parts were continuously shielded with a continuous flow of an inert gas. The process parameters are given

in Table 1. Aluminum wool was added inside of the shielding hood to act as a gas distributor. A visualization experiment using a glycerine mist was conducted to ensure that the inert gas flow coming from the shielding hood covered the complete deposit.

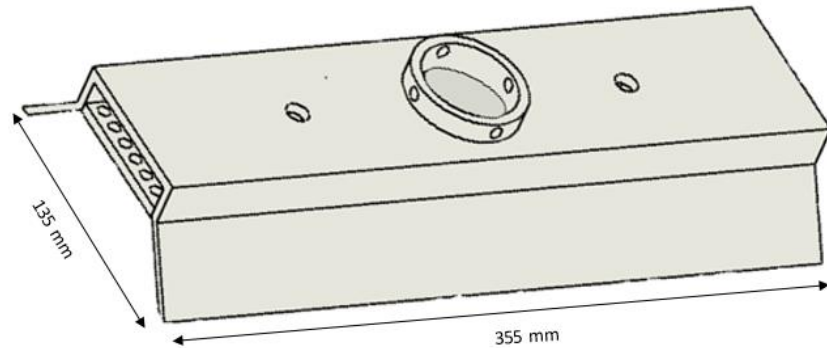


Figure 4 Design of the shielding hood.

Table 1 Test parameters for the PTA-AM system using 17-4PH stainless steel.

Parameter	Range of Parameters
Feed rate	0.42-0.58 g/s (25-35 g/min)
Travel speed	1.3-1.7 mm/s (3-4 in/min)
Current	50-120 A
Voltage	25-28 V
Shield hood gas flow rate	240 kPa (35 Psi)
Center gas	2 lpm
Powder gas	1 lpm
Shield gas	10 lpm
Part Dimensions	
Length of sample	152.4 mm (6 in)
Number of layers	10

### 2.3 Powder Parameters Used for Printing

The 17-4PH stainless steel powders were obtained from two different suppliers; both were argon gas atomized. For Supplier A, the powder was sieved to a size of 53-125  $\mu\text{m}$ , which is ideal for the PTA-AM system, and results in continuous powder flow from the nozzle. The powder size distribution of Supplier B was 45-105  $\mu\text{m}$ . The chemical composition of both powders is given in Table 2. Before the powders were placed in the PTA-AM powder hopper, they were well mixed.

Table 2 Chemical composition of 17-4PH stainless steel powders, wt%.

Element	C	Mn	Si	Cr	Ni	Mo	Cu	S	P	Nb+Ta	O	N	Fe
Supplier A Nominal	0.01	0.2	0.3	16.4	4.1	0.01	4.3	n.d.	0.007	0.3	0.04	0.03	Bal.
Supplier B Nominal	0.07 max	1.0 max	1.0 max	15.0- 17.5	3.0- 5.0	-	3.0- 5.0	0.03 max	0.04 max	0.15- 0.45	0.06 max	0.02 max	Bal.

## 2.4 Operating Parameters for Printing

The 17-4PH stainless steel powders were melted and deposited onto a carbon steel substrate. A range of parameters, given in Table 1, was used to achieve a complete build deposit. The deposit was produced using an oscillation width of 25 mm with an oscillation speed of 15 mm/s. A multi-layered deposit, the sample, was produced for the evaluation of printing.

## 2.5 Characterization of Samples

Each of the 150 mm (6 in) fabricated parts was cut into 2.5 mm (1 in) sections, using a silicon carbide blade. The sectioned samples were hot mounted with a thermosetting phenolic powder for hardness testing and optical imaging. The mounted samples were ground and polished with an EcoMet 250 Buehler grinder/polisher. The samples were first ground using 240, 400, 600, 800 and 1200 grit silicon carbide abrasive papers and then polished using 9, 6, 3, and 1  $\mu\text{m}$  polycrystalline diamond suspension, followed by 0.05  $\mu\text{m}$  alumina suspension. After grinding and polishing, optical and scanning electron microscope (SEM) images were used for microstructural analyses. An Olympus BX-UCB microscope was used for optical imaging and a Zeiss Sigma 300 VP-FESEM was used for SEM imaging. The hardness values of the samples were measured with a Wilson VH3100 hardness machine. A 5x5 hardness matrix was taken over the cross-section of the samples, with indentations 5 mm apart in width and 2 mm apart in height. Vickers hardness values were measured along the width of the sample and across the different layers, using a 1 kg load and a 5 s indentation time.

A tensile test of the unshielded sample was carried out following the ASTM E8 standard. Copper precipitates were imaged and analyzed using transmission/scanning electron microscopy (TEM/STEM) and energy dispersive x-ray (EDX) spectroscopy in a JEOL JEM-ARM 200CF TEM, operated at 200 kV. Extraction replicas were prepared using the following procedure. The sample surface was immersed in Kalling's reagent (copper chloride, ethanol, water and hydrochloric acid) for five minutes to preferentially etch the matrix, so that the precipitates protruded from the surface. A thin layer of carbon was evaporated onto the surface of the etched sample. Squares,  $\sim 2$  mm x 2 mm in size were scribed in the deposited carbon. The sample was then placed back into the etchant, allowing some of the scribed squares to release

from the steel sample and float to the surface. Individual squares were then captured with 3 mm diameter Cu TEM grids. Extracted precipitates, embedded in the carbon film, were ready for imaging in the TEM.

X-ray diffraction (XRD) was used to characterize the microstructure before and after ageing. A Rigaku Ultima IV XRD system was utilized with a Cu x-ray source, operated at 40 kV and 44 mA.

## **2.6 Ageing Process**

The 17-4PH stainless steel requires an ageing heat treatment to precipitate the supersaturated copper; this increases the strength of the material. Depending on the desired strength, hardness and microstructure of the part, the heat treatment of 17-4PH stainless steel can be varied according to Figure 1. Based on the results obtained from as welded samples, samples with the lowest porosity and amount of oxide layers were heat treated at the optimum heat treatment at a temperature of 480°C for 1 h.

## **2.7 Pore Size and Distribution**

Fiji Image J, Version 1.8.0\_172, was used to quantify the porosity in the fabricated parts. All voids in the matrix were marked with a different color than the background in order to determine the void fraction. AM samples were sectioned, mounted, ground and polished and then imaged in the SEM. Each SEM image was analysed and the porosity percentage was determined. This was done on images from multiple locations across each AM sample to ensure an accurate estimation of the porosity.

# **3. Results and Discussion**

## **3.1 Oxide Layer and Porosity**

This work addresses methodologies to reduce or remove oxide layers and voids. Microscopic images identified two types of voids: voids due of the formation of the oxide layers and porosity voids (Figure 5 and Figure 6). The first type of voids was present in the interlayers of the samples. The segregated interlayers were analyzed using energy dispersive x-ray (EDX) spectroscopy. The interlayers had high levels of both chromium and oxygen (Figure 7), which was likely due to the formation of protective  $\text{Cr}_2\text{O}_3$  at the interlayers of the build pieces [20,21]. The oxide layer forms over the 17-4PH deposit, and likely has traces of the stainless steel, as shown in the EDX spectrum (Figure 7). Similarly, the lack of copper can be explained by its absence in the specific region where the EDX analysis was done. Although  $\text{Cr}_2\text{O}_3$  is generally considered to be beneficial from a corrosion perspective, its formation in the interlayers of the AM part acts as a barrier to the continuous formation and development of the internal microstructure, ultimately leading to anisotropic mechanical properties in the fabricated part. Associated with this oxide layer were segregated sections in each of the interlayers, due to poor adhesion that occurs between the oxide layer and the next layer of deposited molten powders. This segregation further intensifies the poor adhesion of the AM part [21]. Analysis of the fracture surface of a tensile sample, produced from one of the sample deposits, indicates that the fractures were initiated along the oxide layers (Figure 8). This illustrates how the oxide layer reduces

the mechanical properties through poor interlayer adhesion. The presence of voids, both in the form of oxide layers between the interlayers and spherical porosity, makes the part heterogeneous and is detrimental to the functionality of the final AM part [7,26].

The other type of voids observed was in the overlays (Figure 5) that formed due to spherical gas entrapment pores and LOF during the welding process [27]. Porosity is typical of AM parts manufactured by different processes and research has been ongoing in an attempt to mitigate them [17]. One such mitigation technique is the use of hot isostatic pressing (HIPing) as a post-welding heat treatment. However, HIPing is a costly and time consuming method [28]. Identifying the different sources of voids in the AM deposits would aid in their mitigation.

The average volume percent of voids present in multiple fabricated parts was determined, for the same operating conditions, to be  $18\pm 2\%$  (Table 1). This high percentage of voids is detrimental in applications with any loading, and as such the parts are required to be fully dense [23]. In order to enhance the densification of PTA-AM parts and to fabricate near net shape products, the two types of voids must be eliminated.

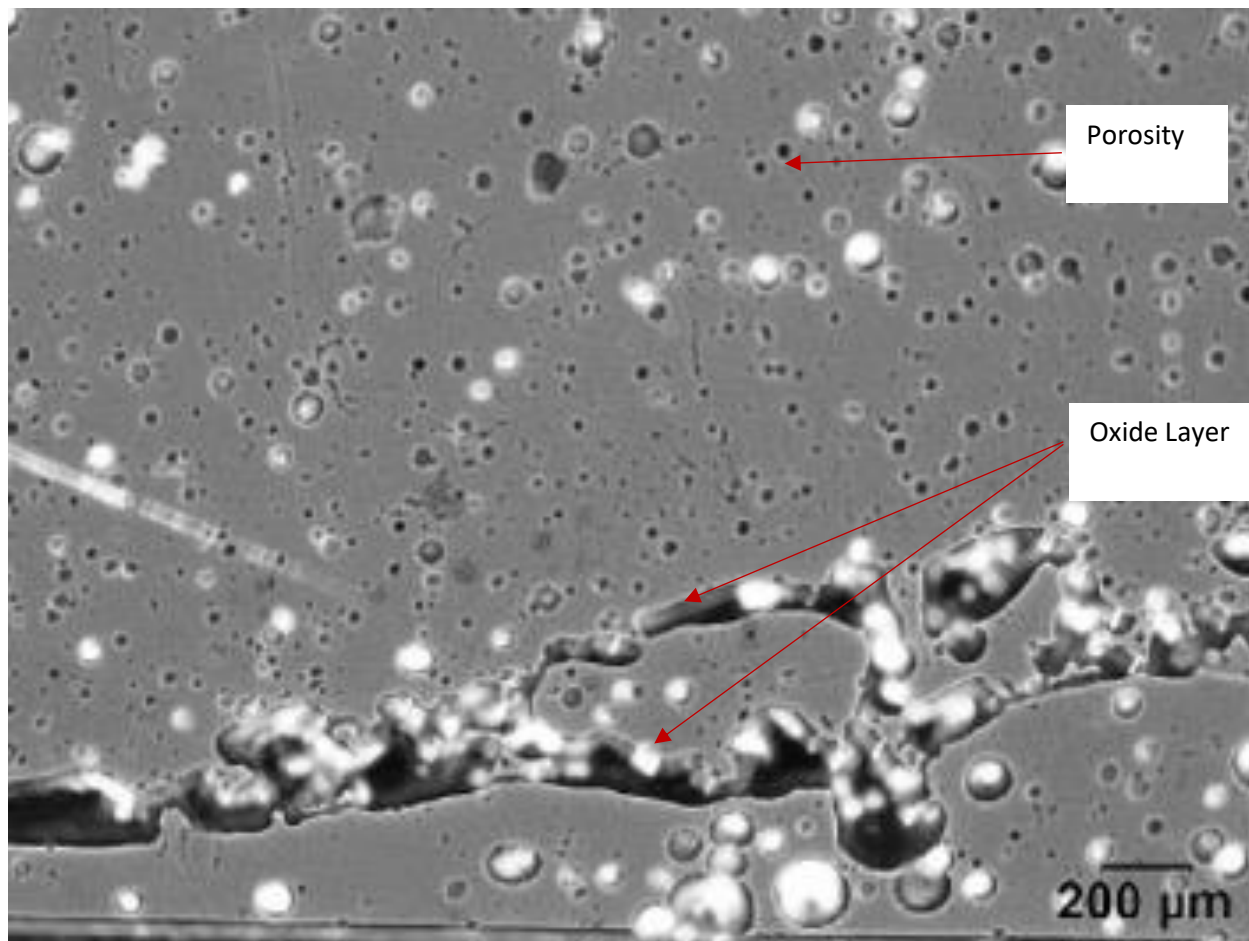


*Figure 5 Optical image showing the oxide layer and porosity.*

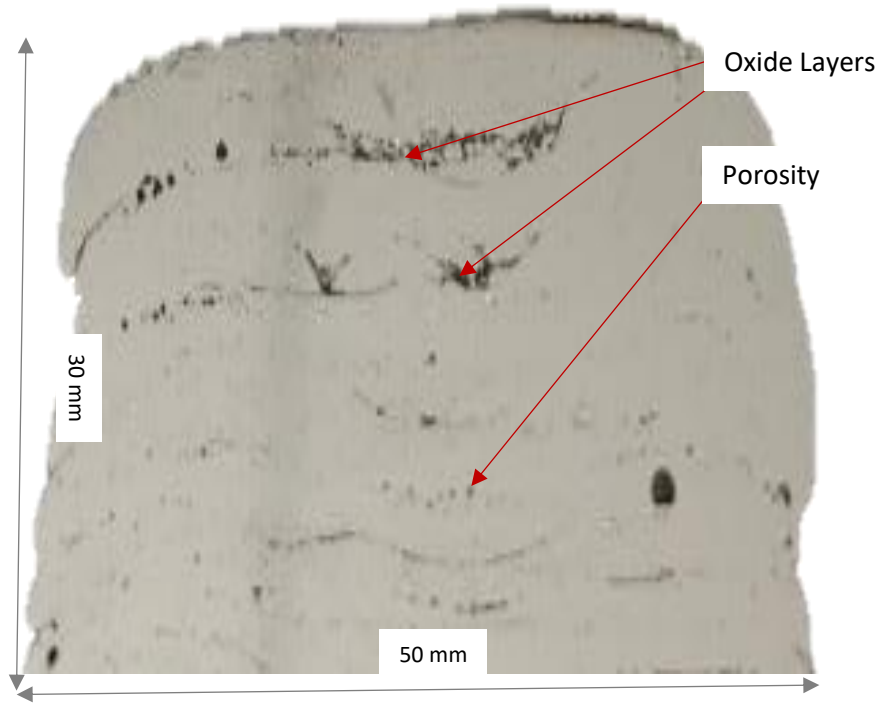


Figure 6 Cross section of deposit showing oxide layers (black transverse lines) and porosity.

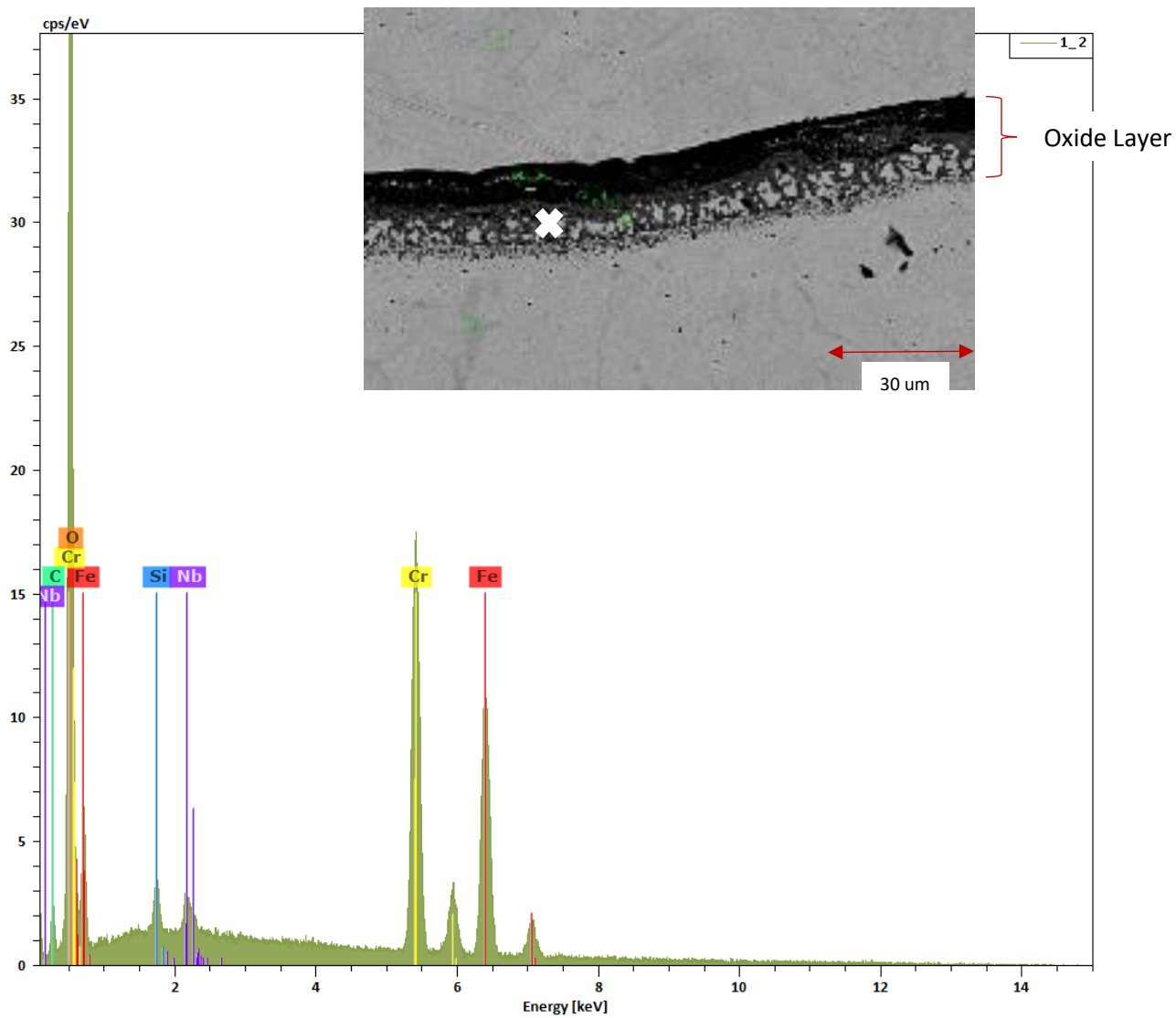


Figure 7 EDX spectrum from the region indicated with an 'X' in the inset image; this region is the oxide layer between two deposited layers.



*Figure 8 Surface of tensile sample showing initiation of cracks along the oxide layers and the brittle fracture of the sample.*

### **3.2 Shielding Hood**

The high level of chromium content in stainless steel is required to enhance the room temperature corrosion resistance of the material. Chromium in the stainless steel reacts with atmospheric oxygen to form an oxide layer on the surface of the stainless steel [20,21]. Even though this process provides the stainless steel with good corrosion resistance, its formation at the interlayers of an AM part has an adverse effect on layer adhesion. Very fast cooling rates in this process mean that the AM part is solidified as the torch is moving; as mentioned earlier, the torch has its own local shielding atmosphere. The  $\text{Cr}_2\text{O}_3$  layer, however, forms if there is no inert shielding atmosphere over the part at temperatures above 947 K. Thus when the torch changes positions and the temperature of the part is at a higher temperature, an oxide layer will form (Figure 6 and Figure 7) [20,21]. In order to prevent the formation of these oxide layers, a shielding hood was designed to ensure the continuous flow of a shielding, inert atmosphere over the AM deposit during processing, preventing the reaction of chromium with oxygen (Figure 4). Samples were fabricated using the same process parameters as in Table 1, with the addition of the shielding hood. The pressure of the shielding hood gas (inert gas pressure) was varied. For the optimum shield gas pressure (Table 1), the volume percent of voids decreased to  $10 \pm 2\%$  (Figure 9). This reduction in voids was correlated to the elimination of oxide interlayers, as shown in Figure 10. Removal of the oxide layers leads to better adhesion and increased densification of the deposit as a whole.

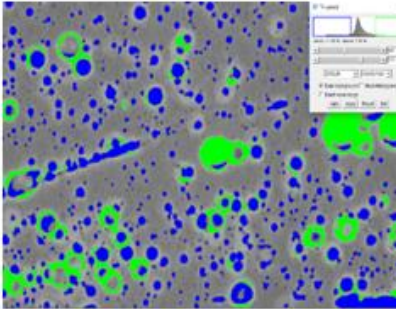
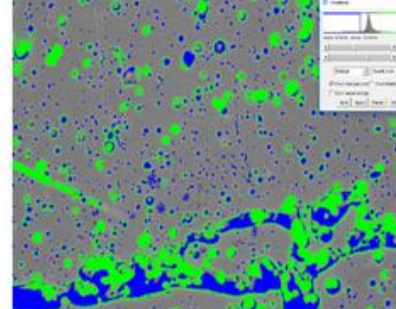
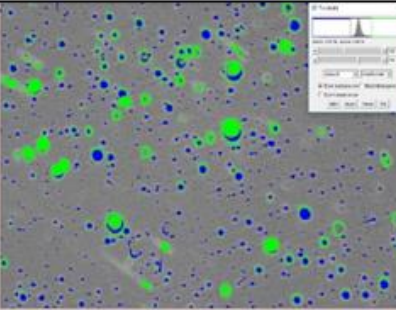
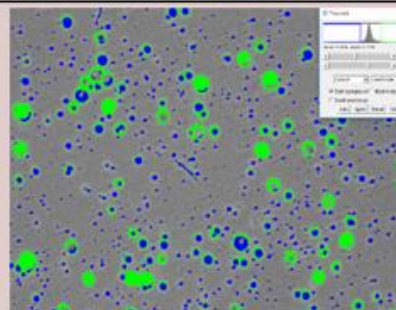
<p><b>Without Shielding</b></p>			<p>Average % of voids: <b>(18±2)%</b></p>
<p><b>With Shielding Hood</b></p>			<p>Average % of voids: <b>(10±2)%</b></p>

Figure 9 Comparison of void percentage (and oxide layer elimination) without (top) and with (bottom) the shielding hood. Both blue and green represent the voids (porosity and oxide layer) present in the part.

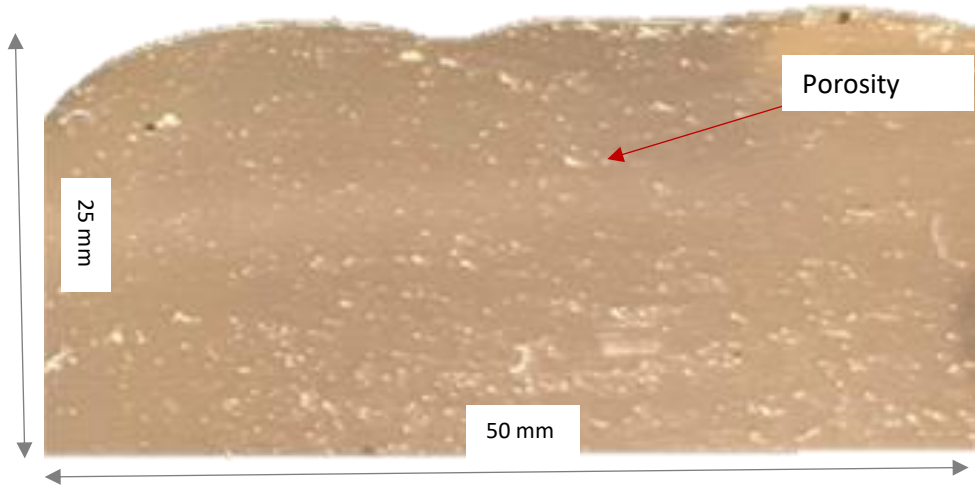


Figure 10 Cross section of deposit showing porosity, but elimination of oxide layers.

**3.3 Process Parameters**

The combination of process, material and operational parameters that yield a dense, near net part is a challenging quest [23,29]. In the PTA-AM system, for example, plasma gas or shield gas flow rate (Table 1) can be used to control the temperature of the weld pool; hence, controlling the cooling rate and the residual stresses generated. Other PTA-AM process parameters, such as the current, voltage or travel speed, can impact the formation of voids inside the deposit and the temperature of the weld pool as well. By reducing the heat input (current and voltage), the part is made more susceptible to the formation of LOF porosity. Similarly, very high travel speeds may not provide sufficient time for complete melting of the powder. Efforts to print a sample required the raising of the heat input, by increasing current or decreasing travel speed, to ensure complete melting of all the powders and the inhibition of the associated internal porosity and, thus, print a part with minimum porosity [23]. For the above reasons, the heat input was increased by almost 15% using the process parameters as shown in Table 3. Higher heat inputs, with and without the shielding hood, resulted in a lower volume percent of internal voids compared with lower heat inputs. With an almost 15% higher heat input, through a combination of increased current and voltage and without the shielding hood, the volume percent of voids dropped from 18% to 8%. Similarly, using the increased heat input and the shielding hood dropped the porosity from 10% to 2%, due to elimination of the oxide layers and LOF porosity. A void volume percent of 2% is still unacceptable in the finished component. Therefore, the source of these voids was investigated.

*Table 3 Parameters for the PTA-AM system using 17-4PH stainless steel.*

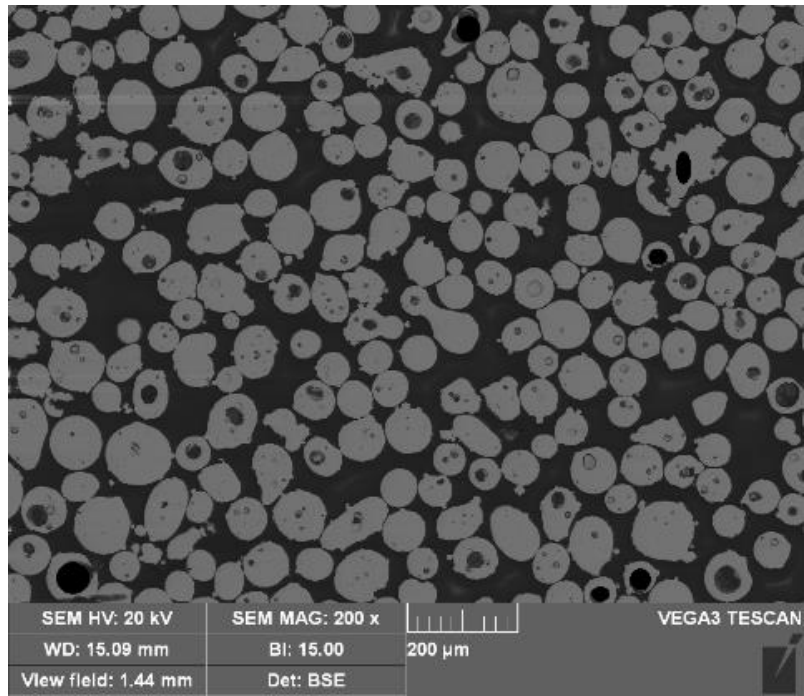
<b>Parameter</b>	<b>Range of Parameters</b>
Feed rate	0.45-0.5 g/s (27-30 g/min)
Travel speed	1.3-1.7 mm/s (3-4 in/min)
Current	110-120 A
Voltage	25-27 V
Shield hood gas flow rate	240 kPa (35 Psi)
Center gas	2 lpm
Powder gas	1 lpm
Shield gas	10 lpm
<b>Part Dimensions</b>	
Length of sample	152.4 mm (6 in)
Number of layers	10

### 3.4 Powder Characterization

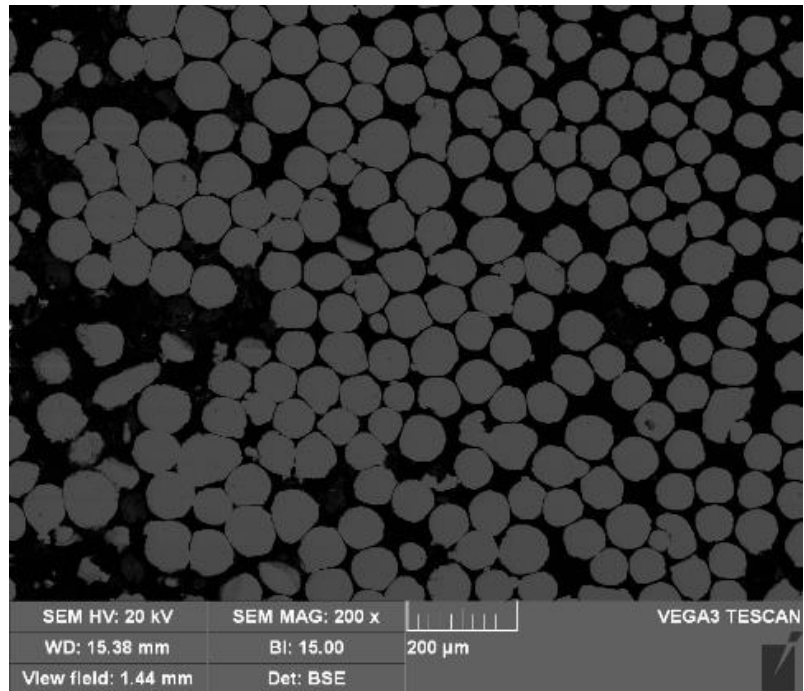
After eliminating the oxide layer and a large number of voids through parameters' optimization and enhanced shielding, the deposits contained approximately 2 volume percent porosity. Haniyeh et al. [23] found that if the initial powders are porous, then there is a greater possibility that porosity will be transferred

to the final fabricated part. The presence of porosity in the powders obtained from the first supplier was analyzed. Image analysis of polished samples of the as received powder indicated that there was almost 9 volume percent porosity present within the powder particles. To determine the effect of internal porosity of powder on the final deposit, new powders (Powder B) were obtained from a different supplier, which had an initial powder porosity of only 0.3 volume percent. Figure 11 shows images of the porosity in both powders.

The deposit formed from the initial powder (Powder A), using the shielding hood and the optimized process parameters (Table 3), had a total void content of 2 volume percent. However, using the new powder (Powder B), the deposit, with identical process parameters and the shielding hood, had an overall void percentage of only 0.4 volume percent. Figure 12 shows sample deposits using Powder A and Powder B, with corresponding images in Figure 13. The influence of powder quality on the homogeneity of the deposit is clearly apparent. Figure 14 shows a cross-section of a sample from the part fabricated with Powder B (Figure 12), using the shielding hood.



(a)

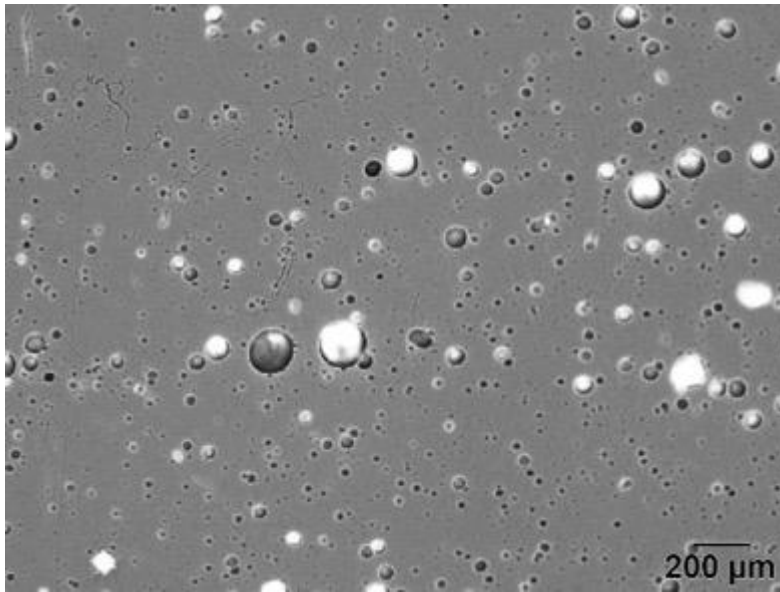


(b)

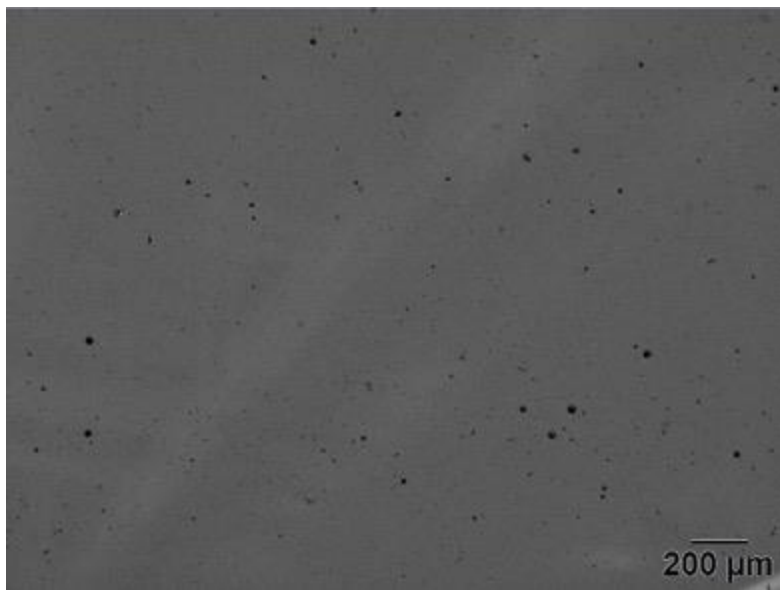
Figure 11 SEM backscattered electron (BSE) images of porosity in powder A (a) and powder B (b).



*Figure 12 View of the surface of samples fabricated with powder A (left) and powder B (right) using identical process parameters.*



(a)



(b)

*Figure 13 Optical microscopy images of parts fabricated with powder A (a) and powder B (b) with identical process parameters.*



Figure 14 Cross section of deposit using powder B showing elimination of both the oxide layers (while using the shielding hood) and porosity.

### 3.5 Hardness

Hardness tests were conducted on all the different samples produced from the different stages of the above experiments. A set of four samples (Table 4) was taken to represent the four main categories of experimentation, and the results are shown in Figure 15. A 5x5 hardness matrix was conducted on each of the samples, and the average results tabulated. All samples were fabricated with the same optimized welding parameters (Table 3); the differences were in the type of powder used and the addition/removal of the shielding hood. It should be noted that there is no obvious effect, within error, of the process variables on the sample hardness (Figure 15). The range of the hardness values for the four samples falls within the range given in the literature for unaged samples, 250-300 Hv [6,8,9]. The error bars represent standard deviation from each set of 25 readings taken per sample.

In order to enhance the hardness of the samples, an ageing heat treatment was conducted at the optimal ageing temperature and time, which was reported to be 480°C for 1 h. Sample D, the sample with the lowest porosity and no oxide layers, was selected from Table 4 to undergo the heat treatment. The build layer does not have an effect on the hardness value. The optimal hardness was achieved following the prescribed quench and temper heat treatment and the results are compared in Figure 16. Clearly, there is a significant increase in hardness following heat treatment.

Table 4 Legend for sample parameters.

Sample ID	Powder Type	Shielding	Porosity/Oxide Layer

A	A	No	Both
B	A	Yes	Porosity
C	B	No	Oxide
D	B	Yes	Neither

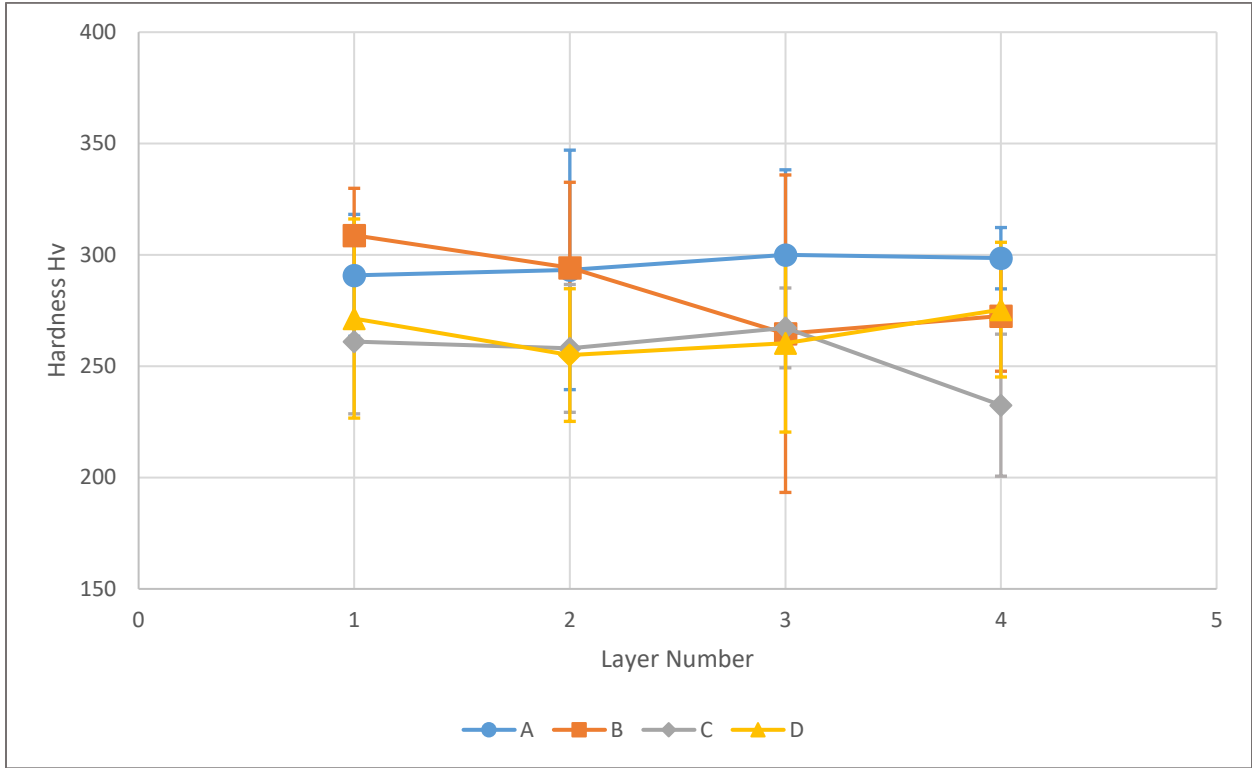


Figure 15 Hardness vs. layer number for samples fabricated with different processing parameters (Table 4)

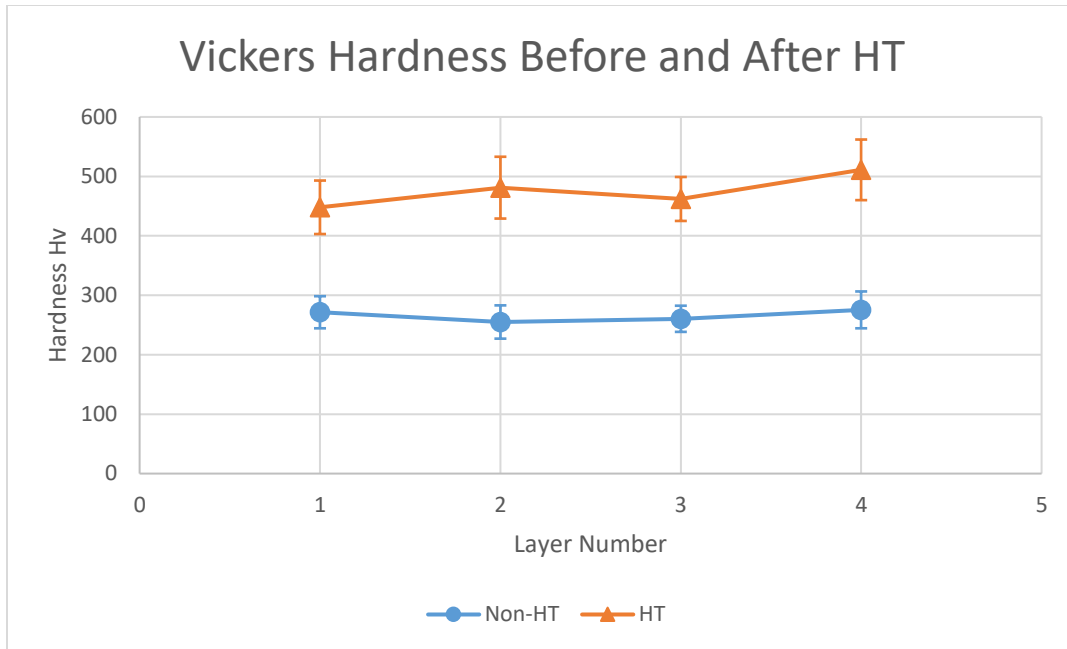
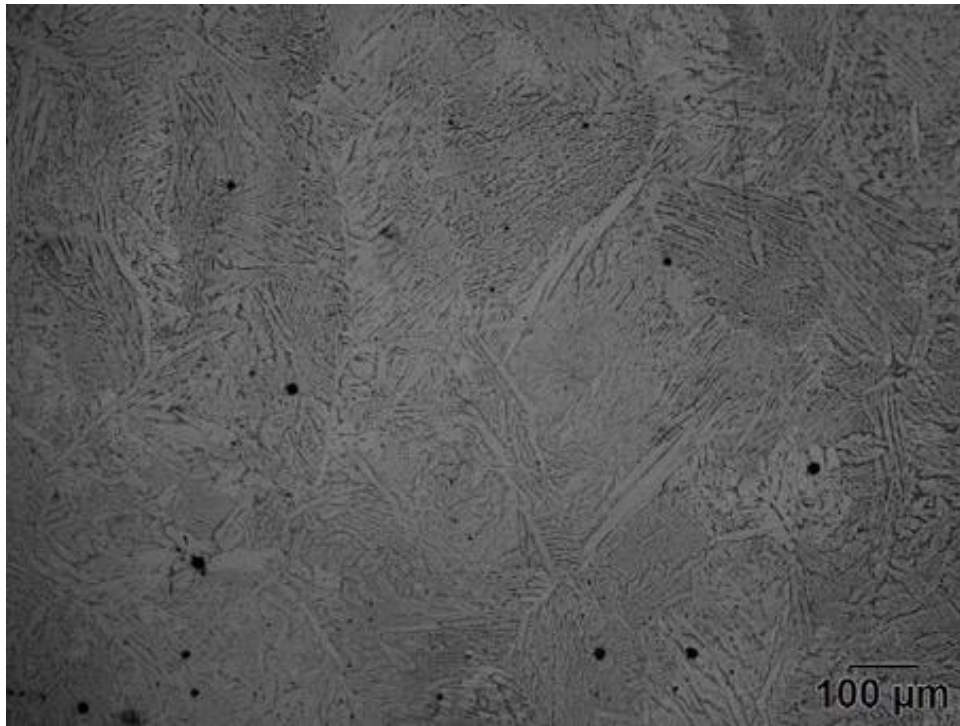


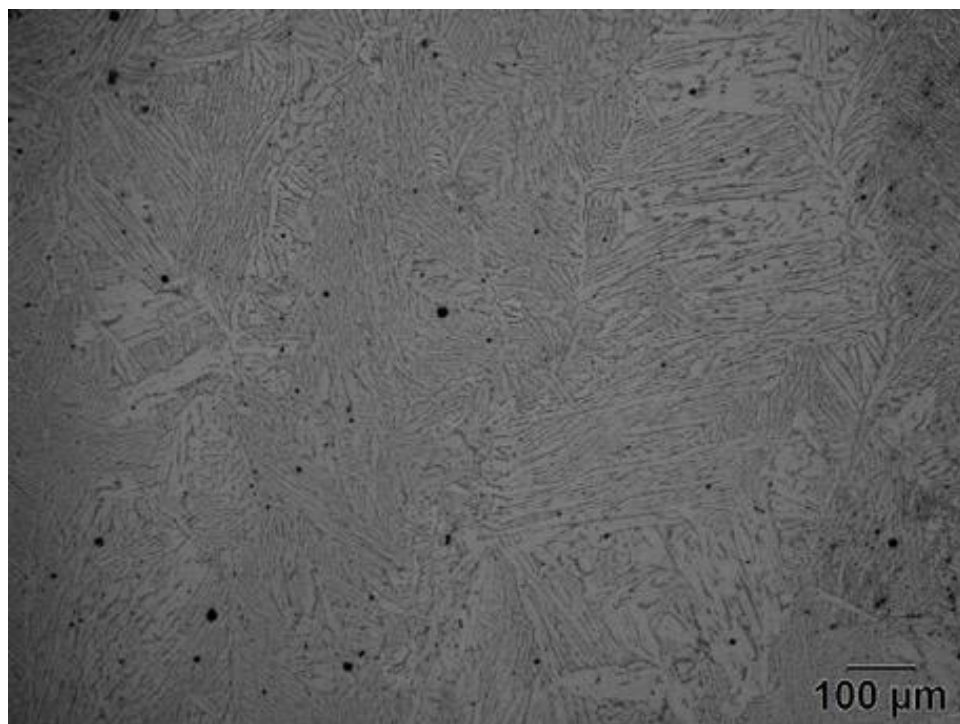
Figure 16 Hardness vs. layer number for non-heat treated (Non-HT) and heat treated (HT) samples after ageing at 480°C for 1 h.

### 3.6 Matrix and Precipitates

In order to understand the effect of the heat treatment on the microstructure of the welded samples, XRD and TEM analysis were conducted. From the literature, the expected matrix of the sample before heat treatment is lath martensite that transforms into tempered martensite after heat treatment [6]. However, because 17-4PH stainless steel has a low carbon content, the differences between lath martensite and tempered martensite (composed of ferrite and very low amounts of cementite) are not discernible using optical microscopy (Figure 17) [30]. XRD was done before and after heat treatment to validate the literature and to differentiate between lath martensite (martensite peaks) and tempered martensite (ferrite peaks). The XRD analysis in Figure 18 for both samples shows peaks which are identified as ferrite peaks, even though the peaks from the first sample were expected to be martensite. This result is due to the low carbon content (0.07 wt.% max.) of 17-4PH stainless steel, which leads to a  $c/a$  ratio close to one for the body-centered tetragonal structure of the martensite [31][32][33][34]. The  $c/a$  ratio is one for a perfect cube, like the body-centered cube structure that forms ferrite. A deviation from one in the  $c/a$  ratio results in a body-centered tetragonal structure, similar to that found in martensite. Additionally, the content of the carbon is further reduced within the matrix because carbon combines with other elements in the stainless steel to form precipitates (Figure 19). Moreover, the almost identical overlap of the XRD peaks before and after the heat treatment, even though copper precipitated, is related to the relative size of the copper atoms to the iron atoms. Copper is present as substitutional atoms in the iron lattice before heat treatment, because the two atoms are similar in size. When the copper precipitates out of the iron lattice, there is little distortion of the iron lattice, so that any shift of the XRD peaks (change in the two theta angle) in the XRD pattern is essentially undetectable. Copper peaks were undetected in XRD after heat treatment.



(a)



(b)

*Figure 17 Optical images for 17-4 PH stainless steel before (a) and after (b) ageing heat treatment for 1 h at 480°C.*

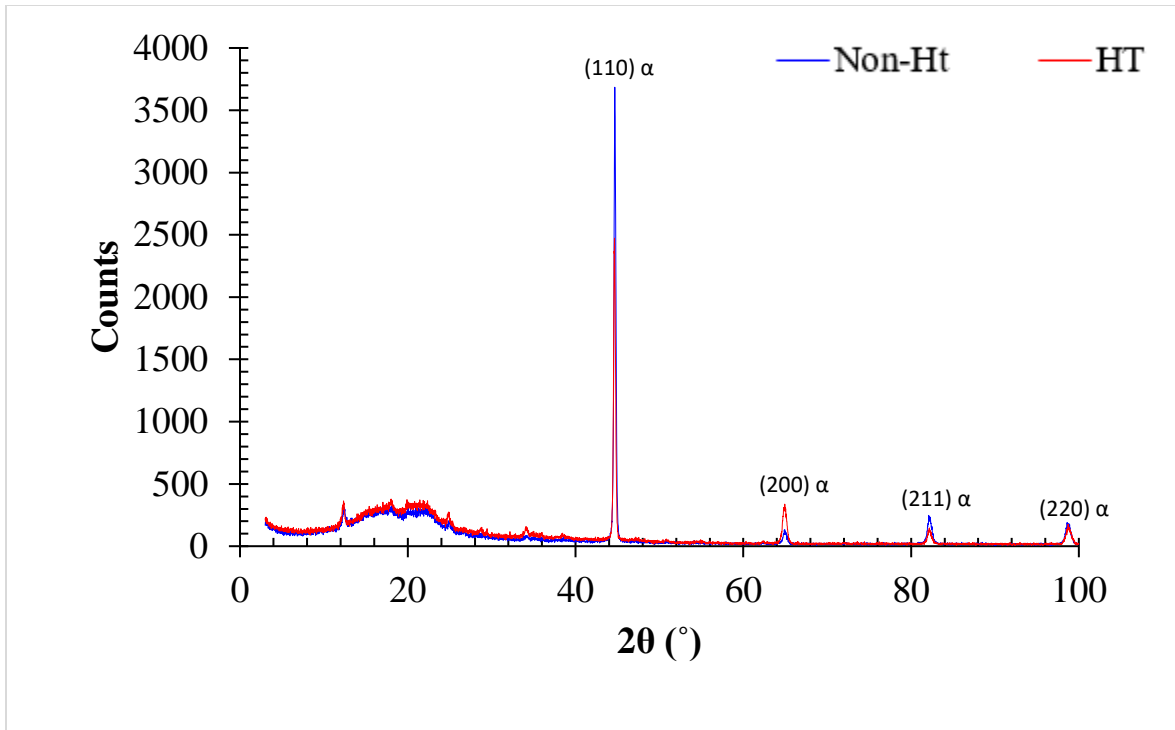


*Figure 18 XRD patterns of heat treated (HT) and non-heat treated (Non-HT) samples.*

TEM analysis was done on extraction replicas to verify that copper precipitated during ageing. STEM bright field (BF) and annular dark field (ADF) images, as well corresponding x-ray maps, of an aged sample are shown in Figure 19. Larger NbC particles are visible, along with small localized copper regions. The copper particles are ~10 nm or smaller in size and can account for the increase in hardness during ageing. The

XRD results showed no change in the matrix and, according to the literature, the precipitation of the copper is the main factor accounting for the increase in the hardness values during heat treatment.

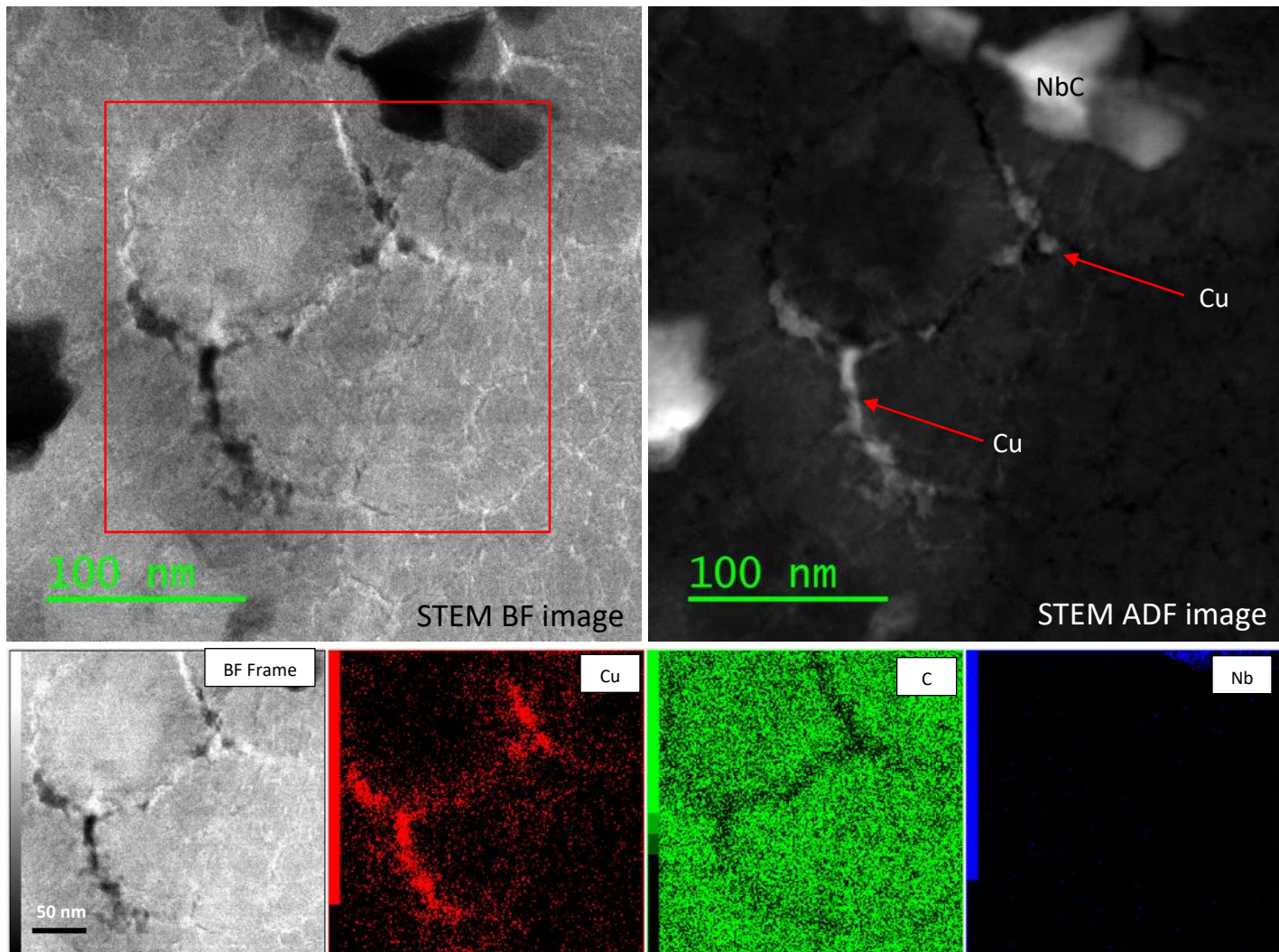
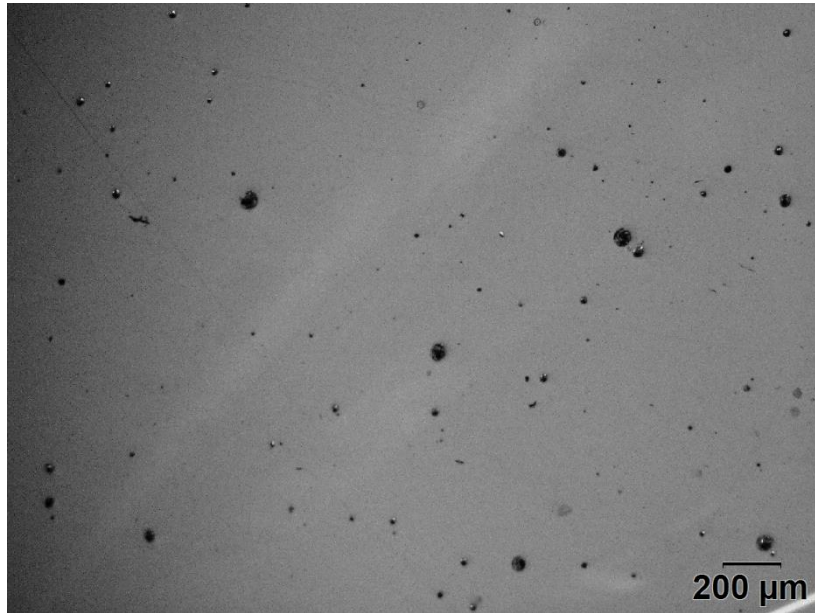


Figure 19 STEM BF image, ADF image and X-ray maps (Cu, C and Nb) of an aged sample; localized regions rich in copper correspond to copper precipitates.

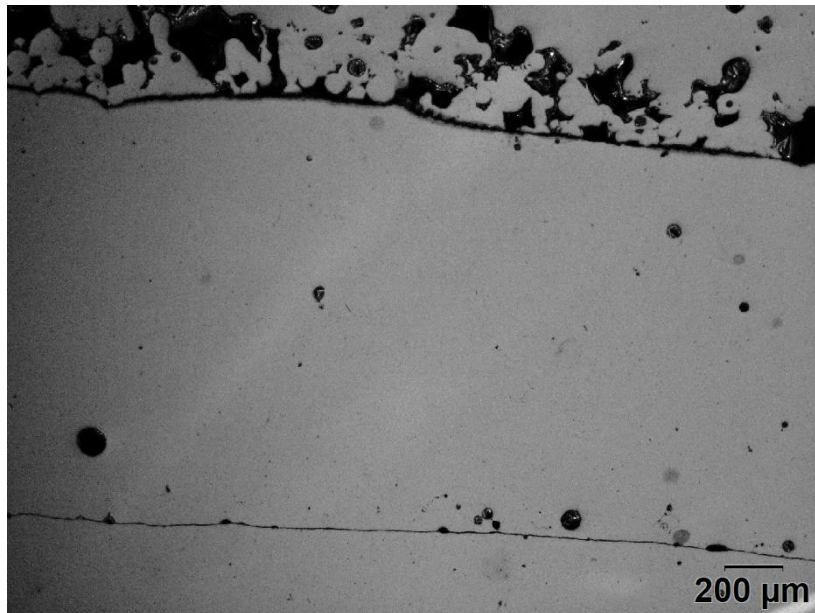
### 3.7 Hydrogen Gas Mix

The shielding hood is an instrument that was designed to verify the mechanism by which the formation of the oxide layer can be completely prevented. After the verification of this mechanism, a mix of 5% H<sub>2</sub>+95% Ar gas was used, without the shielding hood, instead of the pure argon gas with the shielding hood. The gas mix is used to source all the three gases: shield, center and powder. There are several advantages to using this gas mix: removing the oxide layer after it has formed and providing higher heat inputs during welding [35–37]. Because hydrogen is a reducing agent, it reacts with the oxygen in the already formed oxide layer and removes it. Additionally, because the hydrogen in the 5% H<sub>2</sub>+95% Ar gas mix requires higher energy to ionize, as compared to the argon, there is a higher heat input during the welding process

[35]. Hydrogen requires higher energy to ionize because the energy is needed to go into dissociating the hydrogen molecule into two hydrogen atoms. Cross sections from parts built with the 5% H<sub>2</sub>+95% Ar gas mix were compared to samples built with pure argon, without using the shielding hood in either part. It can be seen in Figure 20 (a) that no oxide layers are present in the final part with the 5% H<sub>2</sub>+95% Ar gas mix, which was calculated to have around 0.4% voids, as opposed to 7% voids Figure 20 (b). Without the oxide layers included, Figure 20 (b) has a porosity count of around 0.4%. This verifies that the use of the 5% H<sub>2</sub>+95% Ar gas mix does not attribute to any addition in porosity and is free of any oxides.



(a)



(b)s

*Figure 20 (a) AM part with 5% H<sub>2</sub>+95% Ar gas mix (b) AM part with pure Ar gas*

#### **4. Conclusions**

Several problems were encountered when processing 17-4PH stainless steel using plasma transfer arc additive manufacturing (PTA-AM). Voids were found both at the interface of the interlayers (oxide layers) and within the bulk of a given layer (porosity). The first of these was attributed to the lack of shielding from the atmosphere, resulting in oxygen combining with the chromium present in the 17-4PH stainless steel to form oxide layers. These oxide layers led to poor adhesion between the different layers of the sample. Bulk porosity formation was sensitive to the initial powder quality and process parameters [38]. These two void defects were mitigated as follows:

- The oxide layer was eliminated by the use of a shielding hood, which ensured a continuous, protective inert atmosphere for each layer during deposition.
- Process parameters were optimized by increasing the heat input by up to 15%, which eliminated the formation of lack of fusion (LOF) porosity.
- Pore formation in the bulk layers was traced back to the quality of the powders utilized. Initial porosity in the powders was detrimental to the density and compactness of the fabricated parts. Powders with lower initial porosity produced parts with significantly lower porosity.
- Ageing of the fabricated parts led to an increase in hardness, due to the precipitation of copper nanoparticles.

The hardness of the samples was independent of powder quality, process parameters or layer height. The hardness values coincided with typical values for aged 17-4PH stainless steel. The addition of 5% hydrogen to argon was found to eliminate the formation of oxides, thus eliminating the use of the shielding hood.

#### **5. Acknowledgments**

The authors would like to acknowledge the help and support received from Dr. J. Barry Wiskel, Dr. Ahmed Qureshi and Professor Leijun Li from the University of Alberta. Dylan Rose and Jose Mercado Rojas, Dr. Jonas Valloton and Dr. Abdoul-Aziz Bogno, also from the University of Alberta, are also acknowledged for their help with data analysis, as is Mr. Mike Danysh, at InnoTech Alberta, for assistance with the PTA-AM system. The Natural Sciences and Engineering Research Council (NSERC) of Canada and Syncrude are gratefully acknowledged for funding this project.

## 6. References

- [1] A. Zadi-Maad, R. Rohib, A. Irawan, Additive manufacturing for steels: A review, in: IOP Conf. Ser. Mater. Sci. Eng., 2018: pp. 012–028. doi:10.1088/1757-899X/285/1/012028.
- [2] J.G. Mercado Rojas, T. Wolfe, B.A. Fleck, A.J. Qureshi, Plasma transferred arc additive manufacturing of Nickel metal matrix composites, *Manuf. Lett.* 18 (2018) 31–34. doi:10.1016/j.mfglet.2018.10.001.
- [3] J. Nowacki, Weldability of 17-4 PH stainless steel in centrifugal compressor impeller applications, in: *J. Mater. Process. Technol.*, 2004: pp. 578–583. doi:10.1016/j.jmatprotec.2004.07.117.
- [4] M. Murayama, Y. Katayama, K. Hono, Microstructural evolution in a 17-4 PH stainless steel after aging at 400 °C, *Metall. Mater. Trans. A Phys. Metall. Mater. Sci.* 30 (1999) 345–353. doi:10.1007/s11661-999-0323-2.
- [5] M.R. Tavakoli Shoushtari, M.H. Moayed, A. Davoodi, Post-weld heat treatment influence on galvanic corrosion of GTAW of 17-4PH stainless steel in 3·5%NaCl, *Corros. Eng. Sci. Technol.* 46 (2010) 415–424. doi:10.1179/174327809x409259.
- [6] C.N. Hsiao, C.S. Chiou, J.R. Yang, Aging reactions in a 17-4 PH stainless steel, *Mater. Chem. Phys.* 74 (2002) 134–142. doi:10.1016/S0254-0584(01)00460-6.
- [7] Z. Hu, H. Zhu, H. Zhang, X. Zeng, Experimental investigation on selective laser melting of 17-4PH stainless steel, *Opt. Laser Technol.* 87 (2017) 17–25. doi:10.1016/j.optlastec.2016.07.012.
- [8] G. Yeli, M.A. Auger, K. Wilford, G.D.W. Smith, P.A.J. Bagot, M.P. Moody, Sequential nucleation of phases in a 17-4PH steel: Microstructural characterisation and mechanical properties, *Acta Mater.* 125 (2017) 38–49. doi:10.1016/j.actamat.2016.11.052.
- [9] S. Isogawa, H. Yoshida, Y. Hosoi, Y. Tozawa, Improvement of the forgability of 17-4 precipitation hardening stainless steel by ausforming, *J. Mater. Process. Technol.* 74 (1998) 298–306. doi:10.1016/S0924-0136(97)00286-0.
- [10] U.K. Viswanathan, S. Banerjee, R. Krishnan, Effects of aging on the microstructure of 17-4 PH stainless steel, *Mater. Sci. Eng.* 104 (1988) 181–189. doi:10.1016/0025-5416(88)90420-X.
- [11] M.W. Wu, Z.K. Huang, C.F. Tseng, K.S. Hwang, Microstructures, mechanical properties, and fracture behaviors of metal-injection molded 17-4PH stainless steel, *Met. Mater. Int.* 21 (2015)

- 531–537. doi:10.1007/s12540-015-4369-y.
- [12] B. Song, X. Zhao, S. Li, C. Han, Q. Wei, S. Wen, J. Liu, Y. Shi, Differences in microstructure and properties between selective laser melting and traditional manufacturing for fabrication of metal parts: A review, *Front. Mech. Eng.* 10 (2015) 111–125. doi:10.1007/s11465-015-0341-2.
- [13] E.A. Alberti, B.M.P. Bueno, A.S.C.M. D’Oliveira, Additive manufacturing using plasma transferred arc, *Int. J. Adv. Manuf. Technol.* 83 (2016) 1861–1871. doi:10.1007/s00170-015-7697-7.
- [14] T. Liyanage, G. Fisher, A.P. Gerlich, Microstructures and abrasive wear performance of PTAW deposited Ni-WC overlays using different Ni-alloy chemistries, *Wear.* 274–275 (2012) 345–354. doi:10.1016/j.wear.2011.10.001.
- [15] T. Liyanage, G. Fisher, A.P. Gerlich, Influence of alloy chemistry on microstructure and properties in NiCrBSi overlay coatings deposited by plasma transferred arc welding (PTAW), *Surf. Coatings Technol.* 205 (2010) 759–765. doi:10.1016/j.surfcoat.2010.07.095.
- [16] T.D. Ngo, A. Kashani, G. Imbalzano, K.T.Q. Nguyen, D. Hui, Additive manufacturing (3D printing): A review of materials, methods, applications and challenges, *Compos. Part B Eng.* 143 (2018) 172–196. doi:10.1016/j.compositesb.2018.02.012.
- [17] P.D. Nezhadfar, M. Masoomi, S.M. Thompson, N. Phan, N. Shamsaei, Mechanical Properties of 17-4 PH Stainless Steel Additively Manufactured under Ar and N<sub>2</sub> Shielding Gas, *Solid Free. Fabr. Symp.* (2017) 2430–2446.
- [18] P.H. Huang, M.J. Guo, A study on the investment casting of 17-4PH stainless steel helical impeller of centrifugal pump, *Mater. Res. Innov.* 19 (2015) S977–S981. doi:10.1179/1432891715Z.0000000001924.
- [19] E. Toyserkani, A. Khajepour, S.F. Corbin, A. Khajepour, S.F. Corbin, *Laser Cladding*, CRC Press, 2004. doi:10.1201/9781420039177.
- [20] S.K. Yen, Determination of the Critical Temperature for Forming a Chromium-Rich Oxide on AISI 430 Stainless Steel and Its Corrosion Resistance, *J. Electrochem. Soc.* 143 (2006) 2493. doi:10.1149/1.1837036.
- [21] R. Peter, I. Saric, I.K. Piltaver, I.J. Badovinac, M. Petravic, Oxide formation on chromium metal surfaces by low-energy oxygen implantation at room temperature, *Thin Solid Films.* 636 (2017)

- 225–231. doi:10.1016/j.tsf.2017.06.011.
- [22] J.A. Slotwinski, E.J. Garboczi, Porosity of additive manufacturing parts for process monitoring, in: AIP Conf. Proc., 2014: pp. 1197–1204. doi:10.1063/1.4864957.
- [23] H. Fayazfar, M. Salarian, A. Rogalsky, D. Sarker, P. Russo, V. Paserin, E. Toyserkani, A critical review of powder-based additive manufacturing of ferrous alloys: Process parameters, microstructure and mechanical properties, Mater. Des. 144 (2018) 98–128. doi:10.1016/j.matdes.2018.02.018.
- [24] W.E. Frazier, Metal additive manufacturing: A review, J. Mater. Eng. Perform. 23 (2014) 1917–1928. doi:10.1007/s11665-014-0958-z.
- [25] R. Paul, S. Anand, F. Gerner, Effect of Thermal Deformation on Part Errors in Metal Powder Based Additive Manufacturing Processes, J. Manuf. Sci. Eng. 136 (2014) 031009. doi:10.1115/1.4026524.
- [26] D.F. Susan, T.B. Crenshaw, J.S. Gearhart, The Effects of Casting Porosity on the Tensile Behavior of Investment Cast 17-4PH Stainless Steel, J. Mater. Eng. Perform. 24 (2015) 2917–2924. doi:10.1007/s11665-015-1594-y.
- [27] J.B. Ferguson, B.F. Schultz, A.D. Moghadam, P.K. Rohatgi, Semi-empirical model of deposit size and porosity in 420 stainless steel and 4140 steel using laser engineered net shaping, J. Manuf. Process. 19 (2015) 163–170. doi:10.1016/j.jmapro.2015.06.026.
- [28] W. Tillmann, C. Schaak, J. Nellesen, M. Schaper, M.E. Aydinöz, K.P. Hoyer, Hot isostatic pressing of IN718 components manufactured by selective laser melting, Addit. Manuf. 13 (2017) 93–102. doi:10.1016/j.addma.2016.11.006.
- [29] H.H. Alsalla, C. Smith, L. Hao, Effect of build orientation on the surface quality, microstructure and mechanical properties of selective laser melting 316L stainless steel, Rapid Prototyp. J. 24 (2018) 9–17. doi:10.1108/RPJ-04-2016-0068.
- [30] R.G. Davies, Influence of martensite composition and content on the properties of dual phase steels, Metall. Trans. A. 9 (1978) 671–679. doi:10.1007/BF02659924.
- [31] L. Xiao, Z. Fan, Z. Jinxiu, Z. Mingxing, K. Mokuang, G. Zhenqi, Lattice-parameter variation with carbon content of martensite. I. X-ray-diffraction experimental study, Phys. Rev. B. 52 (1995)

- 9970–9978. doi:10.1103/PhysRevB.52.9970.
- [32] Q. Luo, A New XRD Method to Quantify Plate and Lath Martensites of Hardened Medium-Carbon Steel, *J. Mater. Eng. Perform.* 25 (2016) 2170–2179. doi:10.1007/s11665-016-2053-0.
- [33] R. Schroeder, G. Hammes, C. Binder, A.N. Klein, Plasma debinding and sintering of metal injection moulded 17-4PH stainless steel, *Mater. Res.* 14 (2011) 564–568. doi:10.1590/s1516-14392011005000082.
- [34] Y. Lu, H. Yu, R.D. Sisson, The effect of carbon content on the c/a ratio of as-quenched martensite in Fe-C alloys, *Mater. Sci. Eng. A.* 700 (2017) 592–597. doi:10.1016/j.msea.2017.05.094.
- [35] M. Onsoien, R. Peters, D.L. Olson, S. Liu, Effect of hydrogen in an argon GTAW shielding gas: arc characteristics and bead morphology, *Weld. J. (Miami, Fla.)*. 74 (1995) 10-s.
- [36] A. Durgutlu, Experimental investigation of the effect of hydrogen in argon as a shielding gas on TIG welding of austenitic stainless steel, *Mater. Des.* 25 (2004) 19–23. doi:10.1016/j.matdes.2003.07.004.
- [37] J. Tusek, M. Suban, Experimental research of the effect of hydrogen in argon as a shielding gas in arc welding of high-alloy stainless steel, *Int. J. Hydrogen Energy.* 25 (2000) 369–376. doi:10.1016/S0360-3199(99)00033-6.
- [38] L. Wang, P. Pratt, S. Felicelli, H. Kadiri, P. Wang, Experimental Analysis of Porosity Formation in Laser-Assisted Powder Deposition Process, *TMS (The Miner. Met. Mater. Soc.)* 1 (2009) 389–396. [http://130.18.14.15/publications/docs/2009/02/262128\\_EXPERIMENTAL\\_ANALYSIS\\_OF\\_POROSITY\\_FORMATION\\_in\\_LENS.pdf](http://130.18.14.15/publications/docs/2009/02/262128_EXPERIMENTAL_ANALYSIS_OF_POROSITY_FORMATION_in_LENS.pdf) (accessed May 22, 2019).